

# Controlled release of targeted chemotherapeutic drug dabrafenib for melanoma cancers monitored using surface-enhanced Raman scattering (SERS) spectroscopy

Logan Running, Ricardo Espinal, and Maria Hepel \*

Department of Chemistry, State University of New York at Potsdam, 44 Pierrepont Ave., Stowell Hall, Potsdam, New York 13676, U.S.A.

**Abstract:** The advanced skin cancer melanoma, which is primarily caused by the mutation of BRAF gene, has a high mortality rate and requires high doses of chemotherapeutic drugs. To mitigate the drug toxicity to healthy cells and other side effects, the development of alternative modes of treatment has been extensively sought after. Herein, we describe a new targeted drug delivery system with controlled release, based on nanoparticle nanocarriers functionalized with folate and transferrin ligands for recognition of the respective receptors overexpressed in cancer cell membrane. We have investigated the immobilization of a new drug dabrafenib onto the nanocarriers and its controlled release, aided with surface-enhanced Raman scattering (SERS) spectroscopy which affords ultra-sensitive *in situ* measurement ability owing to the high signal amplification, associated with strong plasmonic fields of the nanocarrier gold nanoparticle (AuNP) cores. The nanocarriers were equipped with Raman reporters: mercaptobenzoic acid (MBA) and para-aminothiophenol (PATP) forming a mixed thiolate monolayer shell on AuNPs. The dabrafenib was covalently attached to MBA via an amide bond which is pH sensitive and enables the drug release at lower pH encountered in cancer cells. This arrangement in the drug binding to the nanocarrier protects the dabrafenib amine group against deactivation until the drug release in the target tumor cells.

**Keywords:** targeted drug delivery; controlled drug release; anti-cancer drugs; dabrafenib; melanoma; SERS; Raman spectroscopy; gold nanoparticles.

## Introduction

Melanoma, a common form of cancer affecting the integumentary system (skin), has the highest mortality rate, 80%, of all skin cancer subtypes <sup>1,2</sup>. The metastatic melanoma carries poor prognosis with an average survival of 10 months <sup>2</sup>. The traditional treatments for melanoma have shown low response of cancer cells (drug resistance develops within months) and severe drug toxicity to healthy cells. Recently, a new promising drug, dabrafenib (DAB), has been approved for treatment of melanoma. In this work, we have investigated a targeted delivery of this drug with controlled release in cancer cells. The targeted delivery of chemotherapeutic drugs has been of considerable interest in view of high toxicity of these drugs to healthy cells and the necessity of administering increased drug doses to destroy resistant cancer tissues <sup>3-5</sup>. The proposed drug delivery system is based on gold nanoparticle (AuNP) nanocarriers functionalized with targeting ligands, folic acid and

transferrin, and covalently attached dabrafenib through a Raman marker linker which enables pH dependent selective drug release in cancer cells. In previous works, we have developed sensitive surface-enhanced Raman scattering (SERS) methods for detecting drug binding to nanocarriers <sup>6</sup> and DNA damage due to mutagenesis <sup>7</sup>.

Dabrafenib is a kinase inhibitor, which selectively inhibits BRAF V600E mutant protein <sup>8</sup>, observed in nearly half of melanomas. The advanced stage melanomas affect also other genes involved in key signaling pathways controlling proliferation, such as NRAS, and NF1 <sup>1</sup>, as well as pathways of replicative telomerase lifespan (TERT) <sup>9,10</sup>. DAB binds selectively to the mutant and inhibits its activity, by taming the proliferation of tumor cells. The normal MAPK (mitogen activated protein kinase) pathway tightly regulates BRAF protein which activates MEK inducing the cell growth. The BRAF mutation occurs when a glutamine is replaced by valine at position 600 in the amino acid sequence.

\*Corresponding author: Maria Hepel

Email address: [hepelmr@potsdam.edu](mailto:hepelmr@potsdam.edu)

DOI: <http://dx.doi.org/10.13171/mjc71/01803171500-hepel>

Received March 4, 2018  
Accepted, March 15, 2018  
Published March 17, 2018

This mutation increases the protein activity by 500-fold compared to the wild type and results in oncogene activity via unregulated MAPK signaling, i.e. it activates the cell proliferation, rather than cell apoptosis, when it is needed. Dabrafenib has been shown to have IC<sub>50</sub> of 0.8 nM in cell-free assays and is 20 times more selective at inhibiting BRAF V600E mutants than the wild type in multiple cancer cells <sup>11-13</sup>. Still the DAB toxicity to healthy cells and various side effects prevent the use of high drug doses required to destroy advanced malignant melanoma. For instance, the DAB therapy is associated with transient elevations in serum aminotransferase, which may lead to acute liver injury. Therefore, the development of a targeted DAB delivery that would affect only tumor cells is highly desirable.

Current studies of cancer theranostic platforms for melanoma treatment include targeted liposomal delivery of vaccine Lipovaxin-MM, a clinical-stage study, Phase I <sup>3,14</sup>; liposomal delivery of oligonucleotides and peptides with BCL-2 targeting <sup>15</sup>, delivery of doxorubicin and combretastatin using liposomes <sup>16</sup> and lipid-polymer hybrid nanocarriers <sup>17</sup>, hybrid NP delivery of TGF $\beta$  inhibitor <sup>18</sup>. Among new promising drugs against melanoma, not tested yet with controlled delivery systems, are two tri-cyclic drugs of the series 2-amino-4-aryl-6-fluoro-4H-benzo[4,5]thieno[3,2-*b*]pyran-3-carbonitrile, where aryl stands for 4-NO<sub>2</sub>C<sub>6</sub>H<sub>4</sub> and 4-FC<sub>6</sub>H<sub>4</sub>, developed by Mouineer et al. <sup>19</sup>. Their IG<sub>50</sub> (concentration of 50% cancer-growth inhibition) for seven different melanoma cell lines are 0.058-0.87 and 0.22-17.3  $\mu$ M, respectively.

In previous studies, we have demonstrated that the surface-enhanced Raman scattering (SERS) spectroscopy can aid in the development of drug delivery systems by providing an ultra-sensitive *in situ* measurement modality for the assessment of the drug loading and releasing dynamics <sup>4,6,20</sup>. The utilization of the high SERS signal amplification, which enables submonolayer drug loading sensitivity, requires the presence of strong plasmonic fields <sup>6,7</sup>. In the system discussed in this work, the nanocarrier AuNP cores afford the necessary plasmonic fields. In addition to that, the self-assembled monolayer (SAM) of thiolates, mercaptobenzonic acid (MBA) and para-aminothiophenol (PATP), deposited on AuNPs, exhibit strong Raman vibration modes, and can serve as Raman probes for monitoring the attachment of drug and targeting ligand molecules. In the proposed nanocarriers, DAB molecules are bound to MBA in the mixed thiolate SAM on AuNPs *via* amide coupling, which enables the drug release at the lowered pH of the cancer cells <sup>21-23</sup>. Further functionalization of the nanocarriers was achieved by using folic acid and transferrin as the cancer-cell targeting ligands. Cancer cells overexpress receptors for folate <sup>24,25</sup> and transferrin protein <sup>26,27</sup>. Therefore, the drug-carrying nanocarriers can recognize cancer

cells and bind to these receptors. Then, they can unload the drug payload, after internalization *via* endocytosis <sup>27-29</sup>, directly in cytosol of cancer cells.

## Experimental

### Materials

The anti-cancer drug dabrafenib (DAB; IUPAC name: N-[3-[5-(2-aminopyrimidin-4-yl)-2-tert-butyl-1,3-thiazol-4-yl]-2-fluorophenyl]-2,6-difluorobenzenesulfonamide, also known as Tafinlar®) was purchased from SelleckChem (Houston, TX, USA). Gold nanoparticles (AuNPs) with a 50 nm diameter coated with a protective citrate monolayer were purchased from Nanopartz (Loveland CO, USA). 4-mercaptopbenzoic acid (MBA) was obtained from Acros Organics (Thermo Fisher Company). A stock solution of 0.1 M MBA was prepared in dimethyl sulfoxide (DMSO), purchased from Alfa Aesar (Tewksbury, MA, USA). N-hydroxysuccinimide (NHS) was purchased from Sigma-Aldrich and 1-ethyl-3-(3-dimethyl-aminopropyl)carbodiimide (EDC) was obtained from ProteoChem. The stock solutions of 0.2 M EDC and 0.1 M NHS were prepared in a 2-(*N*-morpholino)ethanesulfonic acid (MES) buffer with pH of 5.0 and stored at 4°C. Folic acid and 4-aminothiophenol (PATP), and TRIS buffer (tris(hydroxymethyl)aminomethane) were purchased from Sigma-Aldrich. A stock solution of 0.1 M PATP was prepared by adding 0.1 mmol of PATP to 1 mL of DMSO. This solution was refrigerated when not in use.

### Modification of AuNPs with MBA and dabrafenib

Citrate coated gold nanoparticles with 50 nm diameter in DI water were centrifuged at 4000 rpm for 30 min. The supernatant was discarded and the remaining AuNP pellet was dispersed in a 1 mM MBA solution in DMSO. It was set in a shaker for 3 h at 225 rpm and then centrifuged for 30 min at 4000 r.p.m. Then, the supernatant was decanted and the remnant solid was mixed with EDC and NHS solution at pH 5.5. It was set in a shaker for 1 h at 225 r.p.m., followed by centrifugation for 30 min. The supernatant was decanted and the remnant solid was mixed with 1 mM DAB in ethanol and set in the shaker for 18 h at 225 r.p.m. Lastly, the sample was centrifuged for 30 min and the supernatant decanted. The obtained AuNP@MBA/DAB nanocarrier pellet was dried for 5 min in the fume hood and stored at 4°C for analysis by Raman and FTIR-ATR spectroscopy and further experiments.

### Modification of nanocarriers with folic acid and transferrin targeting ligands

A volume of 400  $\mu$ L of AuNP solution (59  $\mu$ g/mL) was centrifuged for 30 minutes and the supernatant was discarded. The AuNP pellet was dispersed in 0.7 mM MBA + 0.3 mM PATP solution in DMSO and set in a shaker for 3 h at 225 rpm. It was then centrifuged for 30 min at 4000 r.p.m. The

supernatant was decanted and the MBA and PATP mixed monolayer-modified AuNPs' pellet (AuNP@MBA,PATP) was mixed with EDC and NHS solution. It was set in the shaker for 1 h at 225 r.p.m., followed by centrifugation for 30 min. The supernatant was removed and the remnant solid was mixed with 1 mM DAB in ethanol and set in the shaker for 18 h at 225 r.p.m., followed by centrifugation for 30 min. The obtained AuNP@MBA,PATP/DAB nanocarrier pellet was then dispersed in a solution of folic acid or

transferrin mixed with EDC + NHS coupling reagents to activate carboxyl groups in these targeting agents for binding to PATP in the mixed thiolate monolayer in AuNP shell. The sample was incubated in a shaker for 18 h at 225 r.p.m., followed by centrifugation and washing with pH 7.4 buffer solution. To make sure that folic acid binds only to PATP and not to MBA ([Figure 1](#)), FA activated with EDC/NHS was added after modification of nanocarriers with dabrafenib.

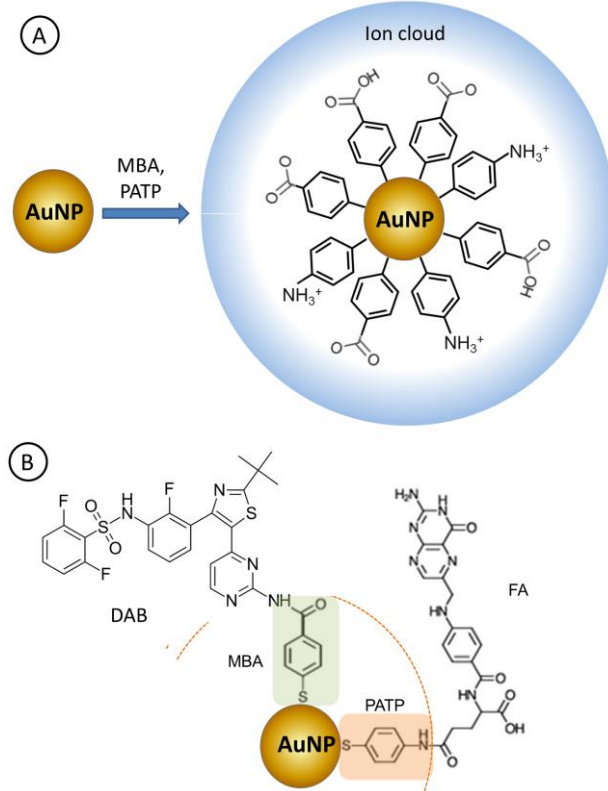


**Figure 1.** (A) Formation of a mixed thiolate self-assembled monolayer of mercaptobenzoic acid (MBA) and para-aminothiophenol (PATP) on AuNPs. (B) A functionalized AuNP@MBA,PATP nanocarrier loaded with anti-cancer drug dabrafenib (DAB) and targeting ligand, folic acid (FA).

## Results and Discussion

### Nanocarrier modification and drug immobilization

The anticancer drug dabrafenib (DAB) was immobilized on AuNP nanocarriers via mercaptobenzoic acid (MBA) linker molecules. The MBA was utilized because it binds to gold surfaces by means of strong thiolate bonds and forms well-ordered self-assembled monolayer (SAM) films on AuNPs. The carboxyl group of MBA exposed to the solution was then used to covalently attach DAB molecules by amide bond formation with DAB's amine group. The strong SERS signals of MBA Raman marker, adsorbed on AuNPs, were used to

monitor the progress of the nanocarrier functionalization and drug loading. This is illustrated in [Figure 2A](#) showing the AuNP@MBA SERS signals at 1586 and 1074 cm<sup>-1</sup> after the MBA-SAM formation (curve 1) and then after the DAB binding to form AuNP@MBA/DAB (curve 2). It is seen that the Raman band intensity at 1586 cm<sup>-1</sup> decreased by 90% due to the masking by DAB, thus confirming the effective DAB binding to the nanocarrier. These results are consistent with previous studies concerning Raman sensors designed for the assessment of DNA damage [7](#), as well as the nanocarrier nanogrid-enhanced SERS probes [6](#), determination of oxidative stress biomarkers [30](#), and the detection of carcinoembryonic antigen [20](#).

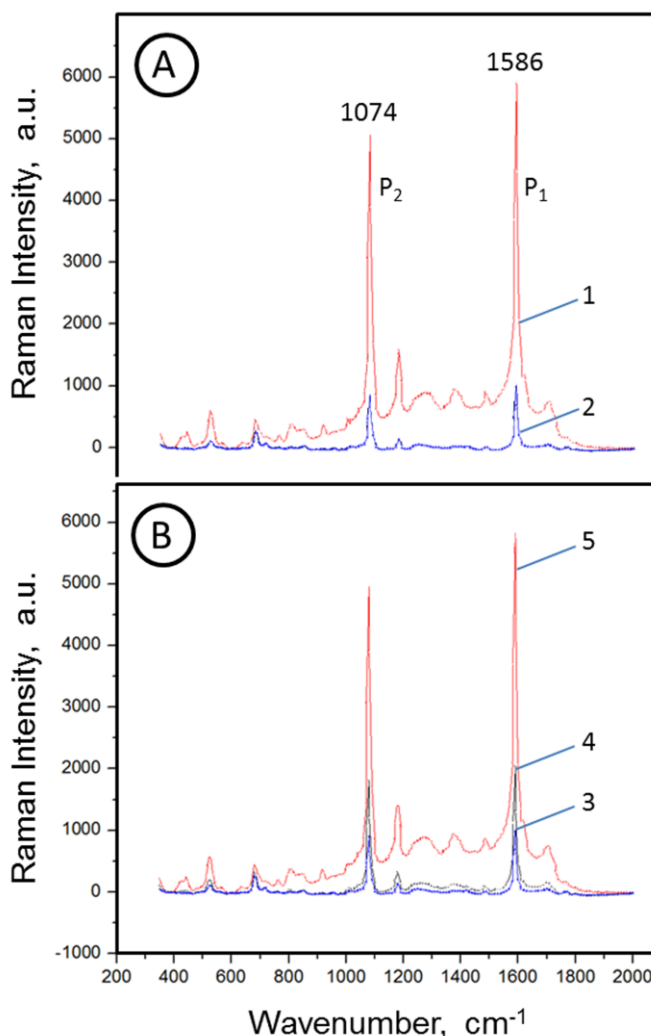


**Figure 2.** (A) Stacked Raman spectra of AuNP@MBA nanocarriers: (1) before drug loading and (2) after immobilization of DAB on nanocarriers. (B) Raman spectra of drug-loaded nanocarriers AuNP@MBA/DAB recorded after soaking nanocarriers in a buffer solution of pH 4.0 for a time period  $t$ : (3) 10, (4) 20, and (5) 30 min, showing an increase of peak intensities due to unmasking of MBA marker caused by the drug release.

To prove that DAB is not simply displacing the MBA from the AuNP surface, we placed the nanocarriers AuNP@MBA/DAB in a buffer solution of pH 4.0, not containing DAB or MBA, to release the DAB molecules from the nanocarrier by acidic hydrolysis of the amide bonds. The obtained SERS spectra are presented in Figure 2B. They show the drug release and unmasking of the underlying MBA-SAM, with almost complete recovery of the SERS signals of MBA. Thus, these measurements

corroborate the effective functionalization of AuNPs and drug loading onto the nanocarriers.

#### **Further evidence of dabrafenib immobilization on modified AuNP nanocarriers**

Further prove of the DAB loading onto the nanocarriers was obtained from FTIR spectroscopy. The analysis of IR spectra of centrifuged pellets of AuNP@MBA/DAB nanocarriers, presented in Figure 3, show the presence of dabrafenib bound to MBA on AuNPs.

The following assignment of the observed vibration modes has been made:  
 $2359\text{ cm}^{-1}$  – C=N-C aromatic stretch;  
 $1739\text{ cm}^{-1}$  – C=O amide stretch (1680-1750) and C=C aromatic bending (1500-1700);  
 $1640\text{ cm}^{-1}$  – C=O amide stretch (1640-1690);  
 $1536, 1561\text{ cm}^{-1}$  – N-H amide bending (1550-1640) – double peak;  
 $1455\text{ cm}^{-1}$  – C=C stretch aromatic (1400-1600);  
 $1365\text{ cm}^{-1}$  – S=O asymmetric stretch in sulfonamide (1335-1375);  
 $1228\text{ cm}^{-1}$  – O=S=O symmetric stretch (1150-1350);  
 $1039\text{ cm}^{-1}$  – S=O sulfoxide stretch (1030-1070).

The contribution of C-F stretch is also likely to be present in the wavenumber range from 1000 to  $1400\text{ cm}^{-1}$ . The absence of the C-N aromatic amine

stretches (1266-1342) indicates on successful binding of DAB to the linker.

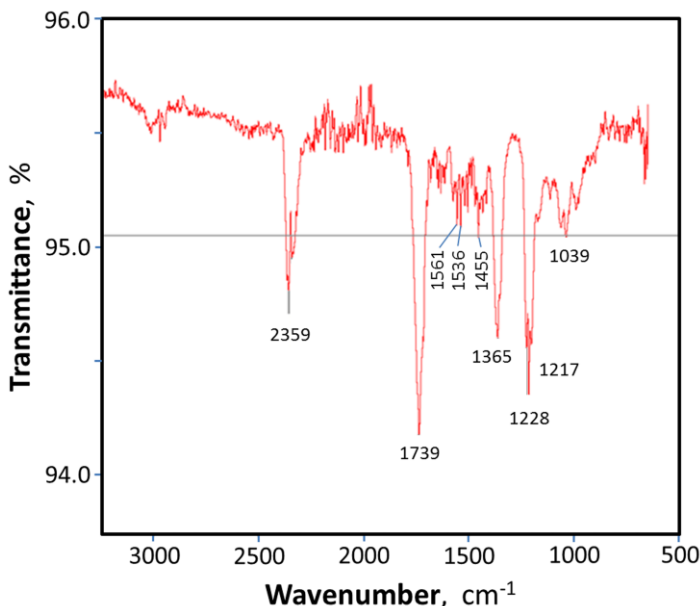


**Figure 3.** FTIR-ATR spectrum of AuNP@MBA/DAB nanocarriers in PBS buffer pH 7.4.

We have also checked if there are any changes of surface plasmon resonance (SPR) band, characteristic of the AuNPs, caused by DAB binding to the nanocarriers. For bare 50 nm diameter spherical AuNPs, the SPR band appears at 530 nm

(Figure 4, curve 1). After binding of DAB to AuNP@MBA, the SPR band shifts to longer wavelengths by *ca.* 100 nm and its intensity is strongly diminished (Figure 4, curve 2).

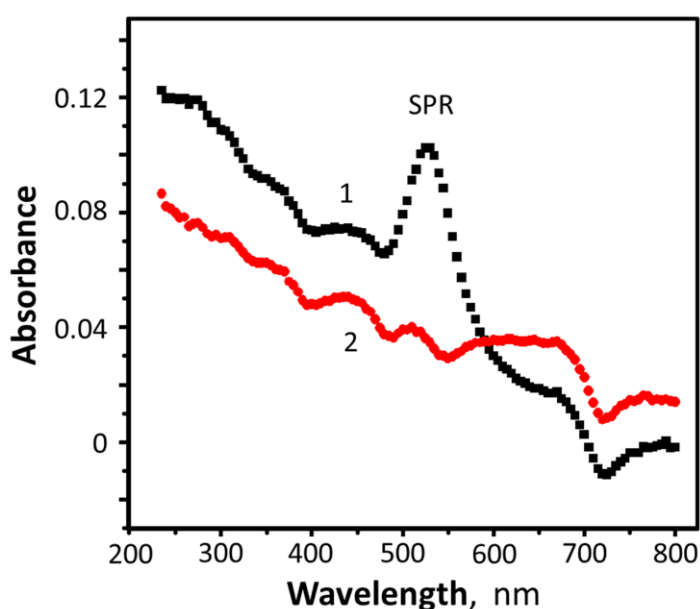


**Figure 4.** UV-Vis absorption spectra for AuNP nanocarriers in TRIS buffer pH 7.4, for: (1) bare nanocarriers, showing a surface plasmon resonance (SPR) band at 530 nm and (2) nanocarriers functionalized with MBA and dabrafenib, showing the red shift and decrease of the SPR band.

#### SERS monitoring of dabrafenib release from AuNP nanocarriers functionalized with folate targeting ligands

The rate of dabrafenib release from AuNP-based nanocarriers functionalized with targeting folate ligands, AuNP@MBA,PATP/DAB,FA, was

investigated using buffer solutions of different pH. The dependences of the relative intensity of the Raman mode at  $1586\text{ cm}^{-1}$  on time of exposure to buffer solutions are presented in Figure 5 for buffers with pH 7.4, 6.0, 5.5., and 4.0.

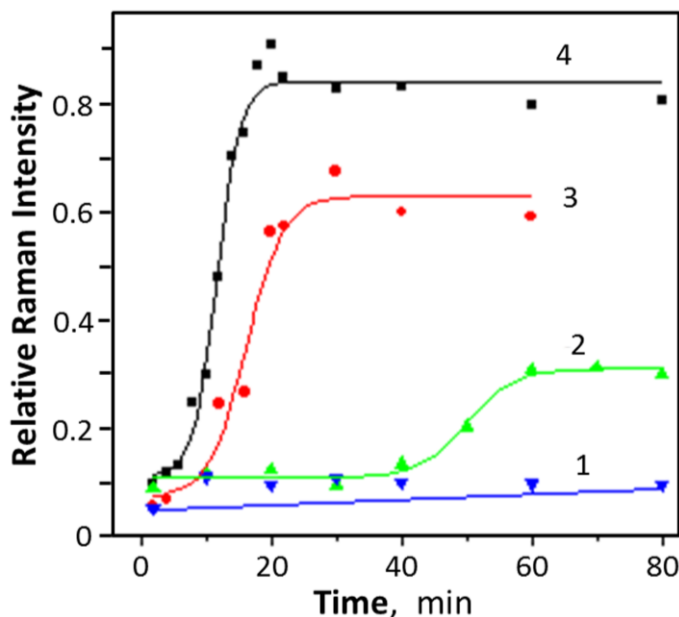


**Figure 5.** Dependence of the relative Raman peak intensity at 1586 cm<sup>-1</sup> for DAB-loaded targeted nanocarriers AuNP@MBA,PATP/DAB,FA on incubation time in buffer solutions with pH: (1) 7.4, (2) 6.0, (3) 5.5, (4) 4.0.

In Figure 5, the relative Raman intensity  $R_{\text{rel}}$  of the Raman mode at 1586 cm<sup>-1</sup> is referred to the intensity of this Raman mode measured for bare AuNP@MBA,PATP nanocarriers without any drugs or targeting ligands attached,  $I_0$ , and Raman intensity for nanocarriers saturated with drugs,  $I_{\text{sat}}$ , according to the equation:

$$R_{\text{rel}} = \frac{I - I_{\text{sat}}}{I_0 - I_{\text{sat}}} \quad (1)$$

It is seen that the initial values of  $R_{\text{rel}}$  are low indicating that the nanocarriers are completely covered with drug molecules and targeting ligands. In a solution of physiological pH 7.4, no change of the Raman peak intensity during the exposure of drug-loaded nanocarriers has been encountered, confirming the high stability of the drug-loaded nanocarriers in this solution. However, in buffer solutions with lower pH, the intensity of the Raman mode at 1586 cm<sup>-1</sup> is increasing with time which means that the dabrafenib molecules are gradually released from the nanocarrier surface, due to the weakening of the amide bond and acidolysis in more acidic media, which results in unmasking of the MBA SAM shell on AuNPs. Note that simultaneously with DAB, the FA is also released

from the nanocarriers due to the same release mechanism but now unmasking the PATP in the AuNP shell. Both MBA and PATP contribute to the intensity of the Raman mode at 1586 cm<sup>-1</sup>, as well as that at 1074 cm<sup>-1</sup>.

#### *Controlled release of dabrafenib using AuNP@MBA,PATP/DAB,TF nanocarriers functionalized with transferrin targeting ligands*

The DAB-loaded nanocarriers functionalized with targeting molecule transferrin (Figure 6A) were also investigated. The mechanism of transferrin binding to the transferrin receptor, overexpressed in cancer cells and exposed in cell membrane, has been broadly studied<sup>26,31,32</sup> due to the importance of iron management and energy production to extensively proliferating cancer cells. To follow the functionalization of AuNPs with transferrin, a calibration curve for the UV-Vis absorption of TF was prepared using transferrin solutions in TRIS buffer, pH 7.4. The absorbance  $A$  increases linearly with increasing TF concentration  $C_{\text{TF}}$ , as illustrated in Figure 6B, according to the calibration equation:  $A = (0.182 \pm 0.005) + (0.0867 \pm 0.001) C_{\text{TF}}$ , for  $C_{\text{TF}}$  in [mg/mL], with high regression coefficient  $R^2 = 0.999$ .

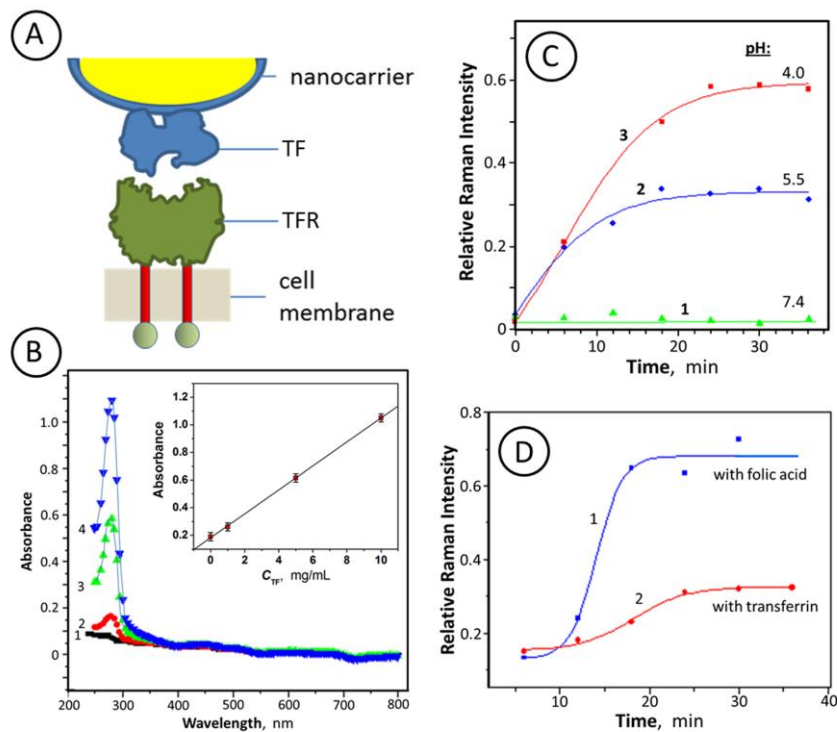


**Figure 6.** (A) Transferrin (TF) functionalized nanocarriers for targeting cancer cells with overexpressed transferrin receptor (TFR). (B) UV-Vis absorption spectra for transferrin in TRIS buffer solutions pH 7.4, with  $C_{\text{TF}}$  concentrations [mg/mL]: (1) 0.0001, (2) 1, (3) 5, (4) 10. Inset: calibration curve of absorbance vs.  $C_{\text{TF}}$ . (C) Temporal evolution of relative Raman signal intensity for MBA + PATP marker vibration mode at  $1586 \text{ cm}^{-1}$  measured during dabrafenib release from transferrin-functionalized AuNP@MBA,PATP/DAB,TF nanocarriers in buffer solutions with pH: (1) 7.4, (2) 5.5, (3) 4.0. (D) Comparison of the DAB release transients with cancer cell targeting by folic acid (1) and transferrin ligands (2) embedded in AuNP nanocarriers; DAB release was carried out in acetate buffer pH 5.5.

The rate of dabrafenib release from AuNP-based nanocarriers functionalized with TF targeting ligands, AuNP@MBA,PATP/DAB,TF, was investigated using buffer solutions of different pH. The dependences of the relative intensity of the Raman mode at  $1586 \text{ cm}^{-1}$  on time of exposure to buffer solutions are presented in Figure 6C for buffers with pH 7.4, 5.5., and 4.0.

Similar to nanocarriers with FA targeting ligands, the AuNP@MBA,PATP/DAB,TF nanocarriers show negligible drug release in a solution of physiological pH 7.4, as no change in the Raman peak intensity is encountered in this solution. It is seen that in solutions with lower pH, the intensity of the Raman mode at  $1586 \text{ cm}^{-1}$  is increasing with time which is indicative of the dabrafenib release and unmasking of the MBA SAM shell on AuNPs. The DAB release from AuNP@MBA,PATP/DAB,TF nanocarriers is slower than that from AuNP@MBA,PATP/DAB,FA nanocarriers and show lower drug release. This is likely due to the large size of transferrin in comparison to folate ligand and obstruction of the drug release process. This is clearly shown of Figure 6D where the release transients are compared for these two types of nanocarriers.

## Discussion

The experiments performed in this work demonstrate the high stability of the drug-loaded nanocarriers, AuNP@MBA,PATP/DAB,FA and AuNP@MBA,PATP/DAB,TF, under physiological pH conditions, since no release of dabrafenib from the nanocarriers was observed and the Raman signals from drug-masked Raman markers remained low during their exposure to solutions of pH 7.4. The stability of drug-loaded nanocarriers under these conditions is essential to prevent any damage to healthy cells and minimize the drug side effects. However, in solutions of lowered pH (5.5 and 4.0), simulating the tumor conditions, an efficient drug release has been observed, as evidenced by the increasing Raman signals from unmasked Raman markers. These results are seen for both folate and transferrin-targeted nanocarriers.

In malignant and cutaneous melanoma, the BRAF mutations are predominant. Tumors with BRAF V600E and BRAF 600K mutations have shown to have worse clinical prognosis than other mutations. The main path of the DAB inhibition mechanism is illustrated in Figure 7, consistent with

the general multi-pathway mechanism of Girotti and Marais<sup>33</sup>. The BRAF mutant, BRAF V600E, activates ERK signaling and promotes tumor cell proliferation and survival. Dabrafenib, transferred to a cancer cell, inhibits the MAPK/RAS pathway<sup>8,11-13</sup> by attaching to BRAF V600E in direct competition with adenosine triphosphate, an energy supplying and phosphorylating molecule. It has been found that dabrafenib is more effective against BRAF V600E mutant than against the wild-type BRAF. Moreover, DAB is also inhibiting other kinases, including: LIMK1, ALK5, NEK11, SIK, PKD2 and BRK. Despite of some selectivity of DAB to the mutated BRAF gene, DAB is still extremely toxic to healthy cells. Therefore, targeted DAB delivery is highly recommended.

Mercaptobenzoic acid, used in this work as the Raman reporter, was attached to gold nanoparticles via a strong thiolate bond. Using EDC/NHS coupling, an amide bond has been formed between the carboxylic acid group on MBA and the amine group of DAB. The Raman scattering peaks for MBA ring vibration modes at 1586 and 1074 cm<sup>-1</sup> have been observed. When MBA is bound to DAB, these vibration modes are masked. After the pH is lowered below 7.4, the amide bonds begin to break releasing the drug. The use of Raman spectroscopy enables temporal monitoring of the increasing intensity of the MBA ring vibration mode. We can

take advantage of the pH sensitivity of the amide bond formed between DAB and MBA to selectively target cancer cells for DAB delivery and treatment of melanoma.

The stability of amide bonds requires more detailed analysis. In general, amides are very stable organic molecules and remain unreactive under different conditions. However, amides will dissociate into the original amine and carboxylic acid under acidic conditions via an SN2 style substitution. The rate of amide hydrolysis is dependent on pH. The lower is the pH, the faster the hydrolysis. Depending on the R-group of the parent carboxylic acid and the R'-group on the parent amine, the hydrolysis could be very slow even at low pH or very rapid, at a higher pH. The amide bond instability is mainly caused by the type of R and R' groups<sup>34</sup>. Hydrolysis of the amide is determined by the nitrogen in the bond to pick up a hydrogen atom and break the bond to the  $\alpha$ -carbon. For this to occur, an amine attached directly to groups which are electron donating, such as nitrogen's imbedded in an aromatic ring, can increase the basic character of the amine. In organic reactions, the electron donating groups generally increase the rate of hydrolysis reactions. On the other hand, having strong electron withdrawing groups on the  $\alpha$ -carbon increases the stability of the carboxylic acid pushing the hydrolysis reaction.

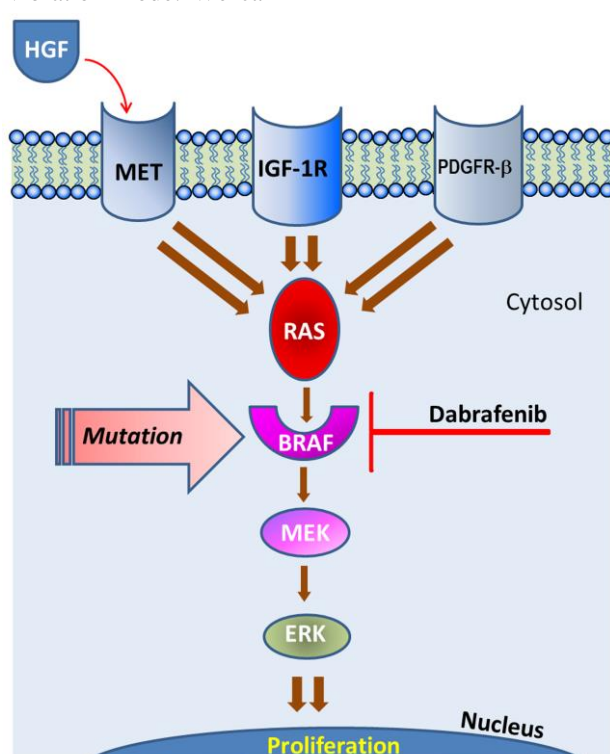
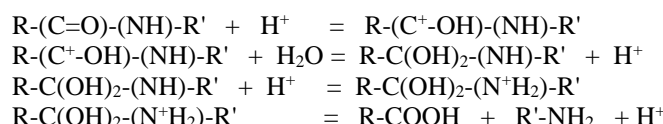


**Figure 7.** Inhibition of BRAF mutant by dabrafenib leading to hindering of uncontrolled proliferation of cancer cells in MAPK signaling pathway. HGF – human growth factor, MET – receptor tyrosine kinase encoded by the MET gene, IGF-1R – insulin-like growth factor 1 receptor, PDGFR- $\beta$  - platelet-derived growth factor- $\beta$ , RAS – cellular signal transduction protein (name from: *rat sarcoma*), BRAF - regulated signal transduction serine/threonine-specific protein kinase, MEK – kinase enzyme which phosphorylates MAPK, ERK – extracellular signal-regulated kinase, MAPK - mitogen-activated protein kinase.

Our drug delivery system relies on amide hydrolysis. The dabrafenib molecule contains a primary amine group that is directly connected to an aromatic pyrimidine ring with two nitrogen atoms.



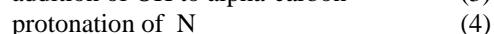
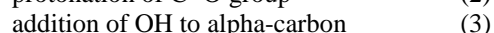
The rapid release of dabrafenib that we have observed in the experiments performed is faster in comparison to other drugs using the same method, such as the gemcitabine <sup>6</sup>, doxorubicin <sup>7</sup>, and azacitidine/decitabine <sup>4</sup>. It is likely that the hydrolysis of the amide bond here is accelerated due to the electron donating nitrogen atoms in the pyrimidine ring adjacent to the amide bond. The presence of electron donating groups may also contribute to the effect of the amide bond twisting which makes it more vulnerable to undergo acidolysis, as suggested by Szostak et al. <sup>35</sup>. On the other hand, the electron withdrawing groups adjacent to the alpha-carbon may stabilize the carboxylic acid component and also promote the amide bond hydrolysis. The drug-loaded nanocarriers, once internalized in cells by endocytosis, may also see an increased rate of amide bond hydrolysis due to the catalysis by nucleic acids <sup>36,37</sup>.

Using folate receptor targeting scheme, an efficient dabrafenib release from the nanocarriers has been achieved. However, when nanocarriers were functionalized with transferrin targeting ligands, considerably lower quantities of drug released were observed, although still a pH dependent release and a short release time were seen. Therefore, this delivery system can still be utilized in practice but with lower efficiency than that based on folate targeting ligand.

## Conclusions

Significant improvement in the efficacy of anticancer drug dabrafenib in melanoma treatment and prevention of damage caused to healthy cells can be achieved using controlled drug delivery nanocarriers functionalized with folic acid and/or transferrin ligands targeting folate/transferrin receptors overexpressed in cancer cells for facilitating endocytosis. Dabrafenib is a kinase inhibitor and is a promising drug for treatment of melanoma, the most prominent skin cancer that currently exists, but its high toxicity to healthy tissues prevents the administration of higher drug doses. Hence, the targeted dabrafenib delivery proposed in this work, may help alleviating toxicity problems in severe cases of melanoma therapy. The application of surface-enhanced Raman scattering spectroscopy enables convenient *in situ* monitoring of dabrafenib loading and release to/from the AuNP-based drug nanocarriers.

This molecular structure induces an efficient release of dabrafenib from MBA functionalized gold nanoparticles. The general scheme of the amide bond hydrolysis is presented below:



## Acknowledgements

This work was supported by Research Collaboration Fund of the SUNY Network of Excellence, RF Project No. 1-114-594.

## Conflict of Interest

The authors declare no conflict of interest.

## References

- 1 - A.H. Shain and B.C. Bastian, *Nat. Rev. Cancer*, **2016**, 16, 345-358.
- 2 - G.V. Long and e. al., *J. Clin. Oncol.*, **2011**, 29, 1239-1246.
- 3 - J. Shi, P.W. Kantoff, R. Wooster and O.C. Farokhzad, *Nat. Rev. Cancer*, **2017**, 17, 20-37.
- 4 - M. Smith and M. Hepel, *Mediterr. J. Chem.*, **2017**, 6, 125-132.
- 5 - T. Santiago, R.S. DeVaux, K. Kurzatkowska, R. Espinal, J.I. Herschkowitz and M. Hepel, *Int. J. Nanomed.*, **2017**, 12, 7763-7776.
- 6 - K. Kurzatkowska, T. Santiago and M. Hepel, *Biosens. Bioelectron.*, **2017**, 91, 780-787.
- 7 - H. Ilkhani, T. Hughes, J. Li, C.J. Zhong and M. Hepel, *Biosens. Bioelectron.*, **2016**, 80, 257-264.
- 8 - A.M. Menzies, G.V. Long and R. Murali, *Drug Des. Devel. Ther.*, **2012**, 6, 391-405.
- 9 - S. Horn and et al., *Science*, **2013**, 339, 959-961.
- 10 - F.W. Huang and et al., *Science*, **2013**, 957-959.
- 11 - J.J. Grob, M.M. Amonkar, B. Karaszewska, J. Schachter, R. Dummer, A. Mackiewicz, D. Stroyakovskiy, K. Drucis, F. Grange, V. Chiarion-Sileni, P. Rutkowski, M. Lichinitser, et al., *Lancet Oncol.*, **2015**, 16, 1389-1398.
- 12 - L. Spain, M.J. M and J. Larkin, *Expert Opin. Pharmacother.*, **2016**, 17, 1031-1038.
- 13 - M. Schreuer, Y. Jansen, S. Planken, I. Chevolet, T. Seremet, V. Kruse and B. Neyns, *Lancet Oncol.*, **2017**, 18, 464-472.
- 14 - US National Library of Medicine. ClinicalTrials.gov, <https://clinicaltrials.gov/ct2/show/NCT01052142?term>.
- 15 - Y.T. Ko, C. Falcao and V.P. Torchilin, *Mol. Pharm.*, **2009**, 6, 971-977.

- 16 - Y.F. Zhang, J.C. Wang, D.Y. Bian, X. Zhang and Q. Zhang, *Eur. J. Pharm. Biopharm.*, **2010**, 74, 467–473.
- 17 - S. Sengupta and et al., *Nature*, **2005**, 436, 568–572.
- 18 - J. Park and et al., *Nat. Mater.*, **2012**, 11, 895–905.
- 19 - A.A. Mouineer, A.F. Zaher, A.A. El-malah and E.A.e.-f. Sobh, *Mediterr. J. Chem.*, **2017**, 6, 165–179.
- 20 - J. Li, Z. Skeete, S. Shan, S. Yan, K. Kurzatkowska, W. Zhao, Q.M. Ngo, P. Holubovska, J. Luo, M. Hepel and C.J. Zhong, *Anal. Chem.*, **2015**, 87, 10698–10702.
- 21 - A. Hulikova, A.L. Harris, R.D. Vaughan-Jones and P. Swietach, *J. Cell Physiol.*, **2013**, 228, 743–752.
- 22 - Y. Kato, S. Ozawa, C. Miyamoto, Y. Maehata, A. Suzuki, T. Maeda and Y. Baba, *Cancer Cell International*, **2013**, 13, 89.81–88.
- 23 - P. Swietach, R.D. Vaughan-Jones, A.L. Harris and A. Hulikova, *Phil. Trans. R. Soc. B*, **2014**, 369, 20130099.
- 24 - J. Sudimack and R.J. Lee, *Adv. Drug Deliv. Rev.*, **2000**, 41, 147–162.
- 25 - R.C. Lynn, M. Poussin, A. Kalota, Y. Feng, P.S. Low, D.S. Dimitrov and D.J. Powell, *Blood*, **2015**, 125, 3466–3476.
- 26 - D.R. Richardson, D.S. Kalinowski, S. Lau, P.J. Jansson and D.B. Lovejoy, *Biochim. Biophys. Acta*, **2009**, 1790, 702–717.
- 27 - K. Ho, H. Li, Z. Qian and H. Sun, *Pharm. Rev.*, **2002**, 54, 561–587.
- 28 - J.J. Turek, C.P. Leamon and P.S. Low, *J. Cell. Sci.*, **1993**, 106, 423–430.
- 29 - Y. Lu and P.S. Low, *Adv. Drug Deliv. Rev.*, **2002**, 54, 675–693.
- 30 - M. Hepel and M. Stobiecka, *J. Photochem. Photobiol. A*, **2011**, 225, 72–80.
- 31 - D.R. Richardson and P. Ponka, *Biochim. Biophys. Acta*, **1997**, 1331, 1–40.
- 32 - E. Ryschich, G. Huszty, H.P. Knaebel, M. Hartel, M.W. Buchler and J. Schmidt, *Eur. J. Cancer*, **2004**, 40, 1418–1422.
- 33 - M.R. Girotti and R. Marais, *Cancer Discov.*, **2013**, 3, 487–490.
- 34 - J.G. Samaritoni, A.T. Copes, D.K. Crews, C. Glos, A.L. Thompson, C. Wilson, M.J. O'Donnell and W.L. Scott, *J. Org. Chem.*, **2014**, 79, 3140–3151.
- 35 - M. Szostak, L. Yao and J. Aubé, *J. Org. Chem.*, **2009**, 74, 1869–1875.
- 36 - B.M. Brandsen, A.R. Hesser, M.A. Castner, M. Chandra and S.K. Silverman, *J. Am. Chem. Soc.*, **2013**, 135, 16014–16017.
- 37 - C. Zhou, J.L. Avins, P.C. Klauser, B.M. Brandsen, Y. Lee and S.K. Silverman, *J. Am. Chem. Soc.*, **2016**, 138, 2106–2109.